Available online at www.sciencedirect.com
SCIENCE DIRECT®
Journal of Catalysis 220 (2003) 486–499
JOURNAL OF CATALYSIS
www.elsevier.com/locate/jcat

Fischer–Tropsch synthesis of hydrocarbons over mesoporous Co/SBA-15 catalysts: the influence of metal loading, cobalt precursor, and promoters

Agustín Martínez,[a,*] Carlos López,[a] Francisco Márquez,[a] and Isabel Díaz [b]

[a] *Instituto de Tecnología Química, UPV-CSIC, Avda. de los Naranjos s/n, 46022 Valencia, Spain*
[b] *Instituto de Catálisis y Petroleoquímica, CSIC, Campus de la UAM, Camino de Valdelatas s/n, 28049 Cantoblanco, Madrid, Spain*

Received 15 April 2003; revised 30 June 2003; accepted 1 July 2003

Abstract

The influence of cobalt loading (10–40 wt% Co), cobalt precursor, and promoters (Re, Mn) on the physico-chemical and catalytic properties of mesoporous Co/SBA-15 catalysts for the Fischer–Tropsch Synthesis (FTS) reaction ($T = 493$ K, $P = 20$ bar, $H_2/CO = 2$) has been investigated. Catalysts were characterized by N_2 and Ar adsorption, X-ray diffraction (XRD), transmission electron microscopy (TEM), X-ray photoelectron spectroscopy (XPS), and temperature-programmed reduction (TPR). For Co/SBA-15 catalysts prepared from Co(II) nitrate the dispersion decreased and the extent of cobalt reduction increased with cobalt loading. A maximum CO conversion was found for the sample with ca. 30 wt% Co loading, though the intrinsic activity of Co remained constant in the range of Co loading studied. More methane and less C_{5+} *n*-paraffins were produced over the less reducible 10 wt% Co loading sample. The addition of ca. 1 wt% Re enhanced the reducibility of cobalt oxides and increased the catalyst activity, though the intrinsic activity of cobalt sites was not altered. Rhenium also favored the formation of long-chain *n*-paraffins (C_{10+}) while decreasing methane selectivity. Promotion of cobalt with ca. 2 wt% Mn significantly improved cobalt dispersion but decreased its reducibility, producing catalysts that were less active than the unpromoted one. At similar cobalt loading (ca. 20 wt%), a much better dispersion and a stronger cobalt–support interaction leading to the formation of low-reducible cobalt silicates was observed for oxidized samples prepared from acetate and acetylacetonate precursors as compared to that derived from cobalt(II) nitrate, as evidenced by TEM, XPS, and TPR. The former catalysts were characterized by a low FTS activity and a product distribution shifted toward the formation of lighter products. Finally, at comparable Co loading Co/SBA-15 catalysts (nitrate precursor) were about 1.5 times more active per weight of total Co than a Co/SiO_2 sample, with only minor differences in product selectivity.

Keywords: Fischer–Tropsch synthesis; Mesoporous SBA-15; Cobalt loading; Catalyst precursor; Rhenium and manganese promotion

1. Introduction

The increasing demand for high-quality and environmentally friendly transportation fuels together with the technological improvements achieved in the last years in gas-to-liquid (GTL) processes making them more efficient and cost competitive has renewed the interest of using natural gas as a potential source of hydrocarbons [1–3]. In particular, diesel fuels made with GTL technology through the Fischer–Tropsch synthesis (FTS) process (synthesis of hydrocarbons from CO and H_2) offers significant environmental and efficiency benefits over those derived from crude oil, as they are mainly composed by linear paraffins having high cetane numbers and are free of sulfur and aromatics pollutants [4,5].

The FTS process was shown to be catalyzed by certain transition metals, with Co, Fe, and Ru presenting the highest activity [6]. Among them, cobalt-based FTS catalysts are usually preferred for the synthesis of long-chain paraffins [7–9], as they are more active per weight of metal, more stable toward deactivation by water (a by-product of the FTS reaction), less active for the competing water-gas-shift (WGS) reaction, and produce less oxygenates than the iron-based systems. Ru-based catalysts are highly active but the high cost and low availability of Ru are important concerns limiting their commercial application [10]. In order to achieve a high density of surface-active sites (Co^0), cobalt precursors are dispersed on porous carriers, with SiO_2, Al_2O_3, and to a lesser extent TiO_2 being the most frequently used. The strength of cobalt–support inter-

* Corresponding author.
E-mail address: amart@itq.upv.es (A. Martínez).

0021-9517/$ – see front matter
doi:10.1016/S0021-9517(03)00289-6

action increases in the order $SiO_2 < Al_2O_3 < TiO_2$. Iglesia et al. [11] showed that at conditions favoring chain growth, i.e., high C_{5+} selectivity, the FT synthesis rates per total Co atoms increase linearly with increasing metal dispersion irrespective of the nature of the support used. In other words, the turnover rates are not influenced by dispersion and support identity, and thus the catalyst activity should be proportional to the number of surface cobalt metal (Co^0) sites. The final density of active Co^0 sites will depend on two main parameters, i.e., cobalt dispersion and degree of reducibility of the supported oxidize cobalt species. Ideally, optimum Co catalysts should be prepared by achieving high dispersions of highly reducible Co species at cobalt loadings as high as possible. For Al_2O_3 and particularly TiO_2 carriers the strong Co–support interaction leads to high dispersions, but also favors the formation of nonreducible cobalt aluminates and titanates, respectively, resulting in a low density of reduced cobalt surface sites. In the case of SiO_2, a weaker interaction of cobalt with the support favors the reducibility of the cobalt oxides but at the same time promotes the agglomeration of cobalt particles during the thermal activation (calcination-reduction) treatments leading to a low dispersion of the Co^0 particles on the silica surface.

The use of periodic mesoporous silicas as supports for preparing Co-based FTS catalysts has been recently explored [12–17]. The very high surface area characteristic of mesoporous molecular sieves should allow for higher dispersions at higher cobalt loading as compared with conventional amorphous silicas. On the other hand, the presence of a uniform pore-size distribution in the ordered mesoporous materials should allow, in principle, for a better control on the cobalt particle size and thus on the catalytic properties. In this line, CoRu/MCM-41 catalysts were reported to be more active for the FTS process at similar metal loading than $CoRu/SiO_2$ while exhibiting similar product selectivities [13]. Recently, the synthesis of a new periodic mesoporous silica, SBA-15, has been reported under acidic medium using triblock copolymers as structure-directing agents [18]. SBA-15 possesses a high surface area (600–1000 m^2/g) and is formed by a hexagonal array of uniform tubular channels with pore diameters ranging from 5 to 30 nm, which are significantly larger than those of MCM-41. Interestingly, SBA-15 also possesses thicker pore walls and better hydrothermal stability than MCM-41 [18,19], a feature that can be relevant for the FTS process in which water is an important by-product. Khodakov and co-workers [15–17] have investigated the effect of pore size in FTS over cobalt-supported on periodic mesoporous SBA-15 and MCM-41 silicas as well as on commercial mesoporous silicas. The FTS reaction rate and C_{5+} selectivity were seen to increase with increasing catalyst pore diameter. These authors found Co/SBA-15 catalysts more active and selective toward C_{5+} hydrocarbons than Co/MCM-41, which was ascribed to a higher reducibility of the larger Co_3O_4 particles formed in the bigger pores of the SBA-15 support [15–17]. However, in a preliminary catalytic study Wang et al. [14] observed a low FTS activity and high methane selectivity for highly dispersed Co/SBA-15 catalysts prepared from cobalt acetate and cobalt acetylacetonate precursors, which was ascribed to a low reducibility of the Co species.

In this work we have undertaken a more thorough study of the characterization of cobalt-supported mesoporous SBA-15 catalysts and their catalytic behavior for the Fischer–Tropsch synthesis reaction. The catalysts are characterized by N_2 adsorption, X-ray diffraction (XRD), transmission electron microscopy (TEM), temperature-programmed reduction (TPR), and X-ray photoelectron spectroscopy (XPS). The influence of cobalt loading (10–40 wt% Co) and cobalt precursor salt (nitrate, acetate, acetylacetonate) and the presence of promoters (Re, Mn) on the physico-chemical and catalytic properties of Co/SBA-15 catalysts were investigated.

2. Experimental

2.1. Preparation of catalysts

The siliceous SBA-15 mesoporous material was synthesized according to the procedure described in Ref. [20] with slight modifications, using Pluronic triblock copolymer (Aldrich, EO_{20}–PO_{70}–EO_{20}, P123) as the structure-directing agent and tetraethyl orthosilicate (TEOS, Merck-Schuchardt) as silica source from a gel of the following molar composition:

$$SiO_2{:}0.0168\,P123{:}5.866\,HCl{:}193\,H_2O.$$

First, the triblock copolymer was dissolved in a solution of water and HCl under stirring, and then the required amount of TEOS was added to the above solution at 309 K and kept under stirring for 20 h. Then, the gel mixture was transferred into polypropylene bottles and heated at 353 K for 3 days in static. After the synthesis, the solid obtained was filtered, exhaustively washed with distilled water until neutral pH, dried at 353 K and finally calcined in a flow of air at 773 K for 6 h to remove the organic template.

Co/SBA-15 catalysts with different Co loading (ca. 10–40 wt%) were prepared by impregnation using a solution of cobalt(II) nitrate (Alpha, 98.9% purity) dissolved in ethanol in excess with respect to the pore volume of the SBA-15 support (liquid/solid ratio of 4 cm^3/g), followed by slow evaporation of the solvent in a rotary evaporator at 323 K and vacuum until dryness. This series of samples was denoted as xCoSBA-n, where x is the nominal Co content (in weight percent) in the calcined catalyst, and n refers to the nitrate precursor. Co/SBA-15 samples containing about 20 wt% Co were also prepared by the above impregnation method but using cobalt(II) acetate (Aldrich, 99% purity) and cobalt(II) acetylacetonate (Acros, 99% purity) as cobalt precursors. These samples were denoted as 20CoSBA-ac and 20CoSBA-aa for cobalt acetate and cobalt acetylacetonate precursors, respectively.

Promoted Co/SBA-15 catalysts were prepared by coimpregnation of the SBA-15 support with an excess of ethanolic solution containing the required amounts of cobalt nitrate (nominal concentration of 20 wt% Co) and promoter precursors. Thus, Re-promoted catalyst was prepared using perrhenic acid (Acros, 85% aq) as precursor, and the sample was denoted as 1Re20CoSBA-n (1 wt% Re nominal content). Mn-promoted catalyst containing about 2 wt% Mn (nominal) was obtained using manganese(II) acetate as precursor (Panreac, pure). This sample was denoted as 2Mn20CoSBA-n. Finally, a Co/SBA-15 sample containing about 20 wt% Co and promoted by both Re and Mn (denoted as 1Re2Mn20CoSBA-n) was also prepared by co-impregnation using an ethanolic solution of cobalt(II) nitrate, perrhenic acid, and manganese(II) acetate as Co, Re, and Mn precursors, respectively.

For comparison purposes, a Co/SiO_2 catalyst containing ca. 20 wt% Co was also prepared by impregnation of a commercial amorphous silica (Fluka, silica gel 100, $S_{BET} = 387\ m^2/g$, $PV = 0.81\ cm^3/g$) with an ethanolic solution of cobalt nitrate as described above for the *x*CoSBA-n samples.

After impregnation, the samples were further dried at 333 K overnight and then calcined in air by increasing the temperature at a controlled heating rate of 1 K/min until 573 K and held at this temperature for 10 h.

2.2. Characterization techniques

The metal content in the calcined catalysts was determined by atomic absorption spectrophotometry in a Varian Spectra A-10 Plus apparatus.

The BET surface area and pore volume of the SBA-15 support and Co-containing catalysts were derived from the corresponding nitrogen adsorption isotherms obtained at 77 K in a Micromeritics ASAP 2000 system. The pore-size distributions were obtained from the Ar adsorption isotherms at 87 K using the BJH method. Prior to the adsorption measurements the samples were outgassed at 473 K for 24 h.

X-ray diffraction patterns were obtained at room temperature in a Phillips X'pert diffractometer using monochromatized Cu-K_α radiation. The average particle sizes of Co_3O_4 in the different catalysts were estimated from the Scherrer equation [21] using the most intense reflexion at $2\theta = 36.9°$. The Co_3O_4 particle sizes in the calcined samples were then converted to the corresponding cobalt metal diameters in reduced catalysts by considering the relative molar volumes of Co^0 and Co_3O_4 using the equation:

$$d(Co^0) = 0.75 \times d(Co_3O_4).$$

Then, the Co^0 metal dispersions can be calculated from the mean Co^0 particle sizes assuming a spherical geometry of the metal particles with uniform site density of 14.6 atoms/nm^2 as described in [22,23] using

$$D = 96/d,$$

where D is the % dispersion and d is the mean particle size of Co^0 in nm.

TEM micrographs were obtained in a JEOL JEM 2000FX microscope operating at 200 kV, equipped with a XEDS detector, and a JEOL JEM 4000EX (structural resolution 0.16 nm and $C_s = 1.0$ mm) transmission electron microscope at 400 kV. For the TEM measurements the solids were dispersed in acetone and dropped on a copper microgrid covered by a holey carbon film.

The reduction behavior of the supported oxidized cobalt phases was studied by temperature-programmed reduction in a Micromeritics Autochem 2910 equipment. About 30 mg of the calcined catalyst was initially flushed with 30 cm^3/min of Ar at room temperature for 30 min and then a mixture of 10 vol% of H_2 in Ar was passed through the catalyst at a total flow rate of 50 cm^3/min while the temperature is increased to 1173 K at a heating rate of 10 K/min. The H_2 consumption rate was monitored in a thermal conductivity detector (TCD) calibrated previously using the reduction of CuO as standard. A different set of experiments was performed in the same equipment to determine the extent of cobalt reduction after submitting the calcined samples to the same reduction treatment applied prior the catalytic tests. For this purpose, about 100 mg of oxidized catalyst was placed in the TPR cell and reduced in situ at 673 K for 10 h at a heating rate of 1 K/min by flowing 50 cm^3/min of a mixture of 10 vol% H_2 in Ar. Then, the temperature was increased from 673 to 1173 K at a rate of 10 K/min and the H_2 consumption registered. The extent of Co reduction was then calculated from the amount of H_2 consumed assuming that complete reduction of Co_3O_4 to CoO and partial reduction of CoO to Co^0 took place during the in situ reduction treatment at 673 K. This assumption is based on the fact that supported Co_3O_4 crystallites have been shown to be reduced to CoO at temperatures typically below 673 K, while higher temperatures are needed to reduce CoO to metallic cobalt [24].

The X-ray photoelectron spectra were obtained with a VG-Escalab-210 electron spectrometer, by using a non-monochromatic Al-K_α (1486.7 eV) source of a twin anode in the constant analyzer energy mode with a pass energy of 50 eV. The spectral acquisition time was also reduced to prevent the damage of the sample. In order to remove charging shifts and deal with Fermi edge coupling problems, binding energies (BE) were scaled against the peak of the C–(C,H) component coming from contamination carbon (set to 284.6 eV). The pressure of the analysis chamber was maintained at 5×10^{-10} mbar.

In situ pretreatments were conducted in a high-pressure gas cell (HPGC) mounted directly to the preparation chamber of the spectrometer, allowing the samples to be transferred into the analysis chamber without exposure to the air after treatments. The analyses were obtained on self-supporting wafers of 9 mm diameter and ca. 5 mg weight that were fixed on a circular sample holder, specially designed for the reaction cell, in such a way that all the reactant

flow passes through the catalyst. The reactant gases (air or a mixture of hydrogen–nitrogen) were introduced into the reaction cell through mass flow controllers at a gas flow rate of 150 cm^3/min. First, the catalyst sample (already calcined at 573 K) was pretreated in situ in flowing air at 150 cm^3/min for 2 h at 623 K, followed by cooling in vacuum to room temperature before acquisition of the XP spectrum. In the next step, the catalyst was again introduced into the HPCG for their reduction in flowing hydrogen (20% in nitrogen) at 150 cm^3/min for 10 h at 673 K and then analyzed.

2.3. Catalytic experiments

The Fischer–Tropsch synthesis reaction was performed in a down-flow fixed-bed stainless-steel reactor ($d_i = 10$ mm, $l = 40$ cm). Typically, the reactor was loaded with 1.0 g of catalyst (0.25–0.42 mm particle size) diluted with CSi (0.25–0.59 mm particle size) up to a constant volume of 6.4 cm^3. Prior to the catalytic experiments the catalysts were reduced in situ at atmospheric pressure by increasing the temperature at a heating rate of 1 K/min up to 673 K and maintained at this temperature for 10 h while passing a flow of pure hydrogen (400 cm^3/min) through the reactor. After the reduction step the temperature was lowered to 373 K under the flow of H_2 and then the reactant gas mixture (H_2:CO:Ar in a volume ratio of 6:3:1, Ar used as internal standard) was introduced at a total flow rate of 250 cm^3/min ($H_2/CO = 2$), corresponding to a GHSV of 13.5 l(NTP)/(g_{cat} h) referred to the syngas feed, and the reactor pressure slowly increased up to 20 bar. Then, the temperature in the catalyst bed was increased from 373 to 493 K at a controlled heating rate of 4 K/min in order to avoid instability of the system induced by the highly exothermic FTS reaction. Once the reaction temperature of 493 K was achieved (TOS = 0), the reaction was led to proceed during a period of 20–24 h to ensure stabilization of the catalyst activity. During the reaction the temperature in the catalyst bed was controlled to 493 ± 1 K by means of two independent heating zones with the corresponding temperature controllers.

During the reaction the reactor effluent passed through a hot trap kept at 473 K and 20 bar to collect waxes, and the stream of products leaving the trap (unreacted H_2 and CO, CO_2, water, alcohols, and hydrocarbons up to C_{15}) was depressurized and analyzed on-line at periodic intervals by gas chromatography in a Varian 3800 chromatograph equipped with three columns and two detectors. Analysis of Ar (reference), CO, CO_2, H_2, and CH_4 was performed using two packed columns, a Porapak Q (0.5 m length) and a 13X molecular sieve (1.5 m length), and a thermal conductivity detector. Alcohols and hydrocarbons from C_1 up to about C_{15} were analyzed using a capillary column (WCOT fused silica, 2.5 m length) and a flame ionization detector (FID). To avoid condensations a controlled flow of nitrogen (50 cm^3/min) was added to the product stream after depressurization while all transfer lines between the reactor and the GC were kept at a temperature of 473 K. Carbon mass balances performed at the end of the experiments including the amount of waxy products collected in the hot trap were quite satisfactory ($100 \pm 2\%$). Preliminary experiments performed in the absence of catalyst showed that the FTS reaction was negligible under the reaction conditions used.

3. Results and discussion

3.1. Characterization of catalysts

3.1.1. Textural properties of Co/SBA-15 catalysts

The N_2 adsorption isotherm for calcined siliceous SBA-15 presented a sharp inflection at a relative pressure in the range of 0.7–0.8 (Fig. 1a) indicative of a good-quality SBA-15 material with uniform mesopores [25,26]. The shape of the N_2 adsorption isotherms of Co-supported samples was similar to that of the original SBA-15 (as an example the isotherms of catalysts containing ca. 20, 30, and 40 wt% Co are shown in Fig. 1 b–d), suggesting that the mesoporous structure of SBA-15 was mostly retained upon cobalt impregnation. The inflection of the adsorption branch of the isotherm occurred at a lower relative pressure (0.65–0.75) for Co-containing samples as compared to the pure silica SBA-15, indicating a decrease of the mean pore diameter after cobalt impregnation. In fact, the mean pore diameter of the pure silica SBA-15 obtained from Ar adsorption at 87 K and using the BJH method was 10.0 nm, while it decreased to about 9.5 nm for the cobalt-containing SBA-15 samples (see inset in Fig. 1). The chemical composition and textural properties obtained by N_2 adsorption of the pure silica SBA-15 sample and supported cobalt catalysts are given in Table 1. The BET surface area and total pore volume of the siliceous calcined SBA-15 (842 m^2/g and 1.18 cm^3/g, respectively) are typical for siliceous SBA-15 synthesized under similar conditions. Both the BET surface area and the total pore volume significantly decreased upon Co impregnation, with the decrease higher at larger Co loading. This may be caused by a partial blockage of the SBA-15 pores by cobalt oxide clusters and/or a partial collapse of the mesoporous structure.

Table 1
Chemical composition and textural properties obtained from N_2 adsorption isotherms of SBA-15-supported Co catalysts

Catalyst	Co (wt%)	Promoters (wt%)		S_{BET} (m^2/g)	Total pore volume (cm^3/g)
		Re	Mn		
SBA-15	–	–	–	842	1.18
10CoSBA-n	9.2	–	–	607	0.83
20CoSBA-n	18.0	–	–	508	0.62
30CoSBA-n	28.7	–	–	421	0.60
40CoSBA-n	40.8	–	–	350	0.49
20CoSBA-ac	17.5	–	–	467	0.62
20CoSBA-aa	16.4	–	–	355	0.55
1Re20CoSBA-n	17.9	0.9	–	498	0.74
2Mn20CoSBA-n	17.8	–	1.8	476	0.76
1Re2Mn20CoSBA-n	17.9	1.3	2.0	443	0.63
$20CoSiO_2$	20.5	–	–	262	0.60

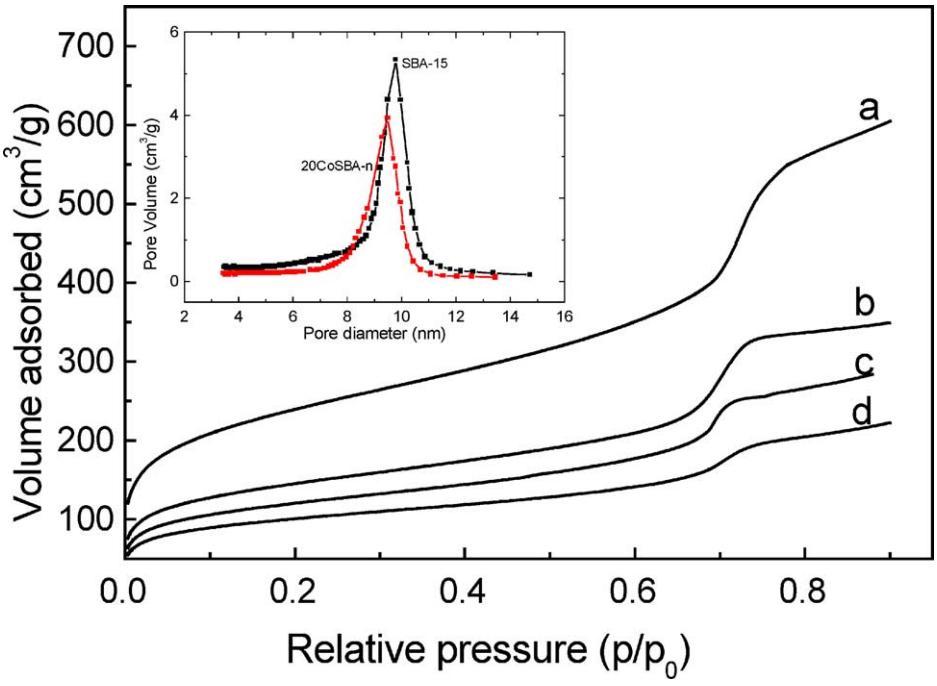

Fig. 1. Nitrogen adsorption isotherms obtained at 77 K for: (a) SBA-15, (b) 20CoSBA-n, (c) 30CoSBA-n, (d) 40CoSBA-n. The inset shows the pore-size distribution for the pure silica SBA-15 and 20CoSBA-n catalysts obtained from Ar adsorption at 87 K using the BJH method.

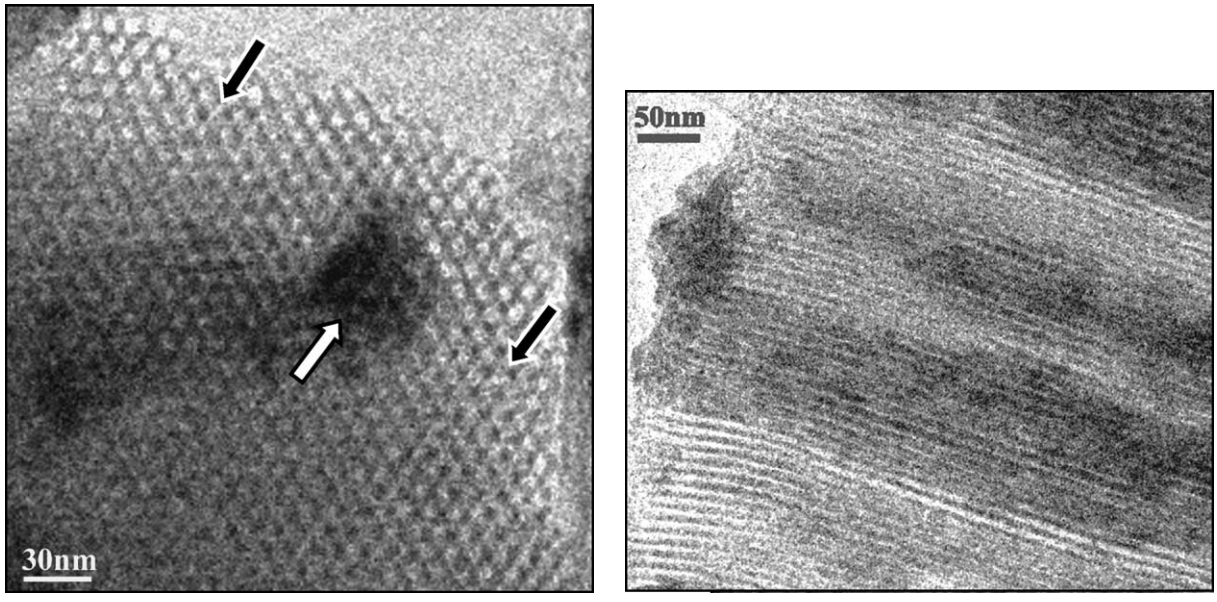

(a) (b)

Fig. 2. TEM images of sample 20CoSBA-n taken along the direction parallel (a) and perpendicular (b) to the *c* axis.

As observed in Table 1, the BET surface area of the Re and Mn-promoted samples was similar to that of the unpromoted catalyst with comparable Co loading. On the other hand, the surface area of the sample prepared from cobalt acetate was slightly lower than that of the equivalent sample prepared from cobalt nitrate, whereas the sample prepared from cobalt acetylacetonate precursor presented a much lower surface area (355 m^2/g). This suggests a higher collapse of the mesoporous structure of the SBA-15 support in the latter catalyst.

3.1.2. Transmission electron microscopy

Cobalt-containing SBA-15 samples were studied by transmission electron microscopy. Micrographs of calcined 20CoSBA-n sample prepared from cobalt nitrate are shown in Fig. 2. Contrast due to the SBA-15 symmetry is observed

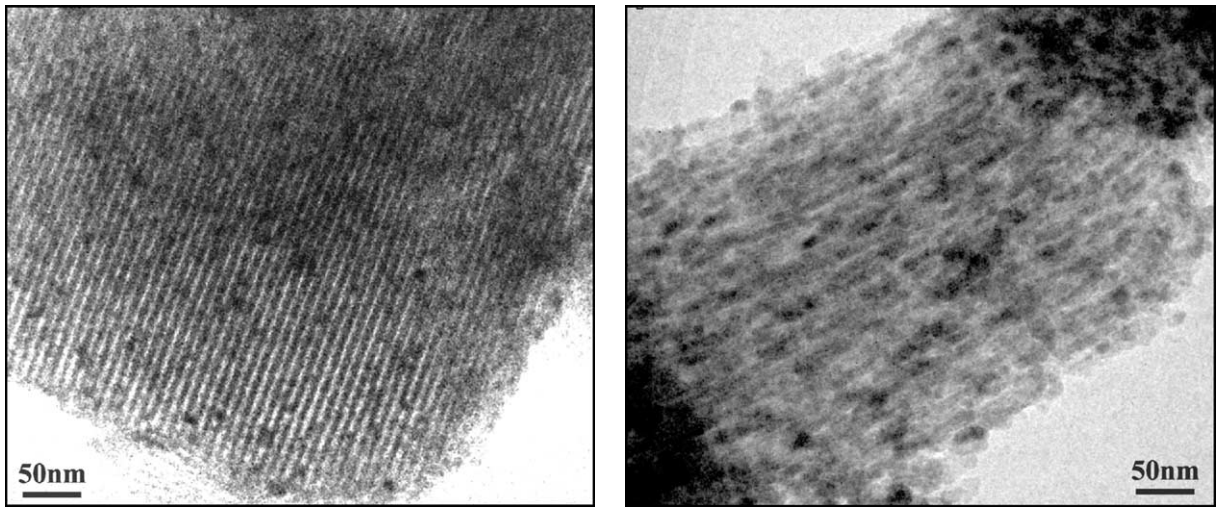

(a) (b)

Fig. 3. TEM images along the direction perpendicular to the *c* axis of sample 20CoSBA-ac.

as well as darker contrast corresponding to cobalt species. Images show the highly ordered hexagonal arrangement of the channels along two directions, parallel (Fig. 2a) and perpendicular (Fig. 2b) to the *c* axis. The SBA-15-type structure was clearly maintained after cobalt impregnation and calcination. The cobalt species were evidenced by darker contrasts and identified by XEDS where the cobalt peak was easily observed. Fig. 2a shows the TEM image of sample 20CoSBA-n taken in the [001] direction, which gives the cross sections of the SBA-15 channels. Two different types of dark contrast from Co particles are apparent. The small dark spots, marked with black arrows, correspond to cobalt oxide located inside the pores. This affirmation is evidenced also by the strong contrast along the longitudinal axis of the crystals in this projection (Fig. 2b). However, it is apparent that not all the channels in this sample are filled by cobalt oxide. The other dark areas, marked with white arrows, give a smeared contrast over the channels, which corresponds to cobalt particles on the external surface.

Micrographs corresponding to the 20CoSBA-ac sample prepared from cobalt acetate precursor are shown in Fig. 3. Although some dark but smeared contrasts, due to cobalt particles located on the external surface of the SBA-15, were observed, images perpendicular to the channel axes of sample 20CoSBA-ac appear to be different than those of sample 20CoSBA-n since no strong contrast along the channel axis was found. On the other hand, as is seen in Fig. 3a, supported cobalt oxide particles appeared to be highly dispersed on the external surface of the 20CoSBA-ac sample. Furthermore, the TEM image of a different particle of the catalyst prepared from cobalt acetate precursor is shown in Fig. 3b. This type of particle, which was not observed in the catalyst prepared from the nitrate precursor, are much different from the typical SBA-15-supported cobalt particles in which the mesoporous structure was clearly seen, and closely resembled a cobalt silicate material. The absence of cobalt oxide particles inside the mesoporous channels might indicate a preferential location of cobalt on the external surface in the acetate sample. However, it can be speculated that after impregnation with the organic salt precursor most of the cobalt species would also be located inside the channels, as it occurs for the nitrate precursor (Fig. 2). Then, during calcination of the impregnated samples the higher temperature required for the decomposition of the organic salt as compared to the nitrate (as we have evidenced from TG-DTA experiments, not shown) may favor a strong interaction of cobalt species with the siliceous wall of the SBA-15 support. Such a strong interaction could prevent migration of cobalt avoiding the formation of large cobalt oxide particles, but it may promote the reaction of the highly dispersed cobalt particles located inside the channels with the silica wall leading to a cobalt silicate-like phase, as observed in Fig. 3b. This explanation seems to be supported by the fact that the cobalt silicate phase appears to be oriented in the direction of the SBA-15 channels.

3.1.3. Structure and particle size of cobalt species

3.1.3.1. X-ray diffraction The XRD patterns of unpromoted and promoted Co/SBA-15 catalysts calcined at 573 K as well as those of the bulk Co_3O_4 spinel phase are presented in Fig. 4. All catalysts prepared from cobalt nitrate precursor (Fig. 4 b–e) showed the reflexions characteristic of the Co_3O_4 spinel. In this series of samples the peaks become narrower, indicating an increase of the mean Co_3O_4 crystallite size, when increasing the Co content. Co_3O_4 particles large enough to be detected by XRD appeared to be also present in the sample prepared from cobalt acetate (Fig. 4f), although the intensity of the corresponding reflexions was much lower than that of the catalyst prepared from cobalt nitrate with equivalent Co loading (Fig. 4c), suggesting that most of the cobalt in the acetate sample should be highly dispersed on the SBA-15 surface. On the other hand, no

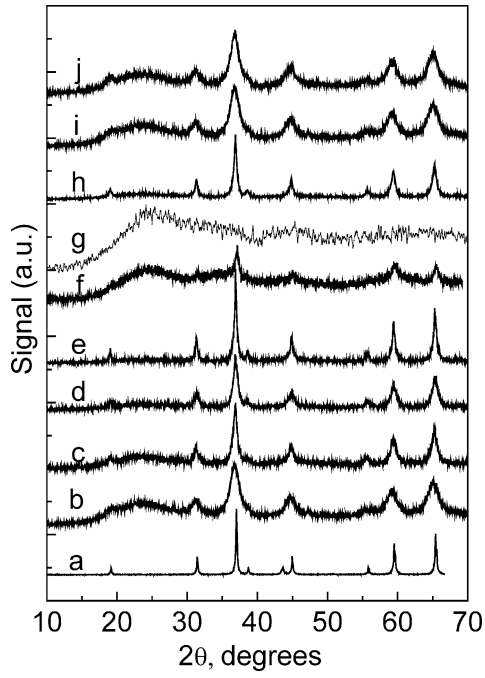

Fig. 4. X-ray diffraction patterns for unpromoted and promoted Co/SBA-15 catalysts and bulk Co_3O_4: (a) Co_3O_4, (b) 10CoSBA-n, (c) 20CoSBA-n, (d) 30CoSBA-n, (e) 40CoSBA-n, (f) 20CoSBA-ac, (g) 20CoSBA-aa, (h) 1Re20CoSBA-n, (I) 2Mn20CoSBA-n, (j) 1Re2Mn20CoSBA-n.

crystalline cobalt phases were observed in the sample prepared from cobalt acetylacetonate (Fig. 4g), reflecting also a very high dispersion of the cobalt in this sample. Similarly, Sun et al. [27] did not observe any Co diffraction peak for a Co/SiO_2 sample (10 wt% Co) prepared from cobalt acetate, and concluded that Co should be highly dispersed on the silica surface. In a recent work, Wang et al. [14] did not find any diffraction peaks in calcined Co/SBA-15 catalysts prepared from cobalt acetate with Co loading up to 20 wt%, which was taken as evidence of the formation of nanosized Co_3O_4 clusters inside the mesopores of the SBA-15. Similar results have been reported by Yin et al. [12] for Co/HMS mesoporous catalysts with Co loading up to 15 wt%. However, the absence of Co_3O_4 reflexions in supported Co catalysts does not necessarily imply the presence of very small C_3O_4 particles escaping XRD detection, but could also be due to the formation of a noncrystallized cobalt phase induced by a strong cobalt–support interaction. This would be more so in the case of the catalysts prepared from the organic cobalt precursors which are known to decompose at higher temperatures than cobalt nitrate, thus facilitating a strong Co–support interaction. We will come to this point later when discussing the XPS and TPR results.

The mean Co_3O_4 crystallite sizes calculated using the Scherrer equation are presented in Table 2. The average Co_3O_4 crystallite size in the unpromoted *x*CoSBA-n series showed a clear dependence on the cobalt loading, with larger particles being formed at higher loading. Thus, at 10 wt% Co loading the mean diameter of Co_3O_4 was 6.2 nm, and it increased up to 17.6 nm for the sample loaded with ca. 40 wt% Co. It must be noted that the mean Co_3O_4 crystallite diameter exceeded the pore diameter of the SBA-15 support (about 10.0 nm as determined from Ar adsorption) for Co loading above 20 wt%, indicating that larger Co_3O_4 particles are located on the external surface of the SBA-15 support. This is in fact observed by TEM, as discussed before. For the promoted samples containing about 20 wt% Co, the addition of small amounts of Re slightly decreased the mean Co_3O_4 crystallite size, while a significant reduction of the average size of Co_3O_4 particles from 11.4 to 5.9 nm was noted upon the incorporation of ca. 2 wt% Mn. Moreover, the catalyst promoted by both Re and Mn showed a mean Co_3O_4 diameter intermediate (6.8 nm) between that of Re- and Mn-promoted samples. The corresponding Co^0 dispersions estimated from XRD as described under Experimental are given in Table 2.

3.1.3.2. X-ray photoelectron spectroscopy: calcined catalysts Fig. 5 illustrates the Co2p XP spectra obtained for the different catalysts after calcination at 573 K for 10 h, and the corresponding spectral parameters are collected in Table 2. No other peaks, either from cobalt or from the siliceous SBA-15 carrier, were split or broadened, indicating the absence of differential charge effects. First, the series of unpromoted *x*CoSBA-n catalysts (nitrate precursor) will

Table 2
Physico-chemical properties of cobalt phases in Co/SBA-15 catalysts as determined from XRD, TPR, and XPS characterization techniques

Catalyst	XRD		Extent of Co	BE of $Co2p_{3/2}$ (eV)	
	Co_3O_4 crystallite diameter (nm)	Co^0 dispersion (%)	reduction[a] (%)	Calcined	Reduced
10CoSBA-n	6.2	20.5	27	781.8	781.9
20CoSBA-n	11.4	11.2	62	780.4	778.8
30CoSBA-n	13.8	9.3	88	–	–
40CoSBA-n	17.6	7.3	89	780.2	778.0
20CoSBA-ac	–	–	28	781.8	–
20CoSBA-aa	–	–	12	782.0	–
1Re20CoSBA-n	9.5	13.5	83	780.9	778.5
2Mn20CoSBA-n	5.9	21.7	40	780.4	778.7–781.5
1Re2Mn20CoSBA-n	6.8	18.8	84	–	–
$20CoSiO_2$	14.1	9.1	89	–	–

[a] Estimated from TPR after reducing the samples in diluted H_2 (10 vol% H_2 in Ar) at 673 K for 10 h and assuming reduction of CoO to Co^0.

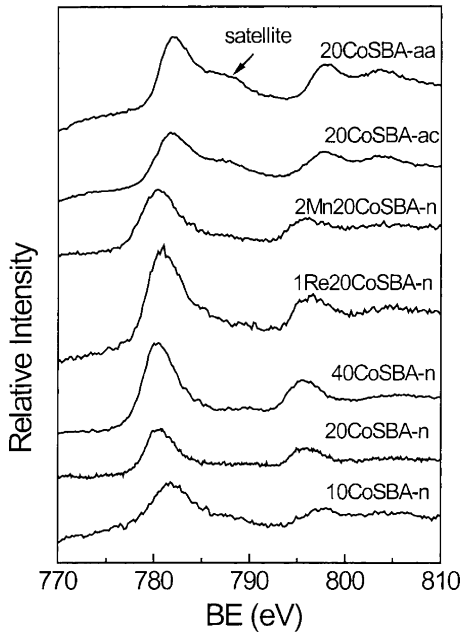

Fig. 5. Co2p core-level spectra of calcined unpromoted and promoted Co/SBA-15 catalysts.

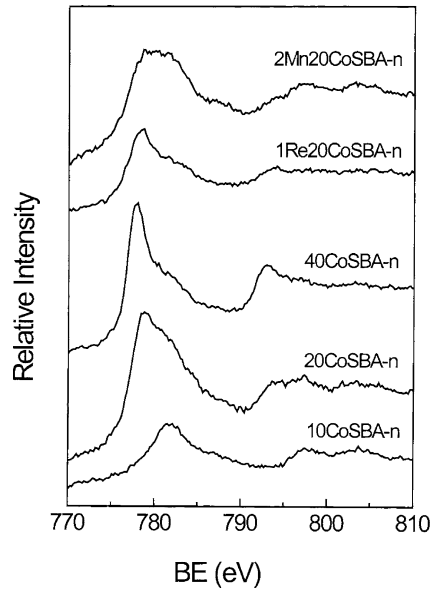

Fig. 6. Co2p core-level spectra of the Co/SBA-15 catalysts after in situ reduction in flowing hydrogen (20% in nitrogen, 150 cm^3/min) at 673 K for 10 h.

be analyzed. Samples with Co loading of ca. 20 and 40 wt% are characterized by binding energies of the $Co2p_{3/2}$ component of 780.4 and 780.2 eV, respectively, and a low intensity of the shake-up satellite peak at ca. 787 eV, which is typical for Co^{2+}/Co^{3+} ions in the Co_3O_4 spinel phase [28]. Therefore, Co_3O_4 is the predominant cobalt phase in these catalysts after calcination at 573 K. In the case of the catalyst with low Co loading (10CoSBA-n) the $Co2p_{3/2}$ peak was shifted toward higher energies (BE = 781.8 eV), and the relative intensity of the shake-up satellite slightly increased with respect to the high-loaded samples. These features are indicative of the presence of Co^{2+} species in octahedral symmetry as found in CoO [29] and can be taken as evidence of a strong interaction of the cobalt species with the surface of the SBA-15 support. However, the full-width half-maxima (FWHM) of the $Co2p_{3/2}$ peak was found to be higher (4.3 eV) than that expected if octahedral Co^{2+} ions were the only cobalt species formed, suggesting the presence of another Co component at lower BE that could be related to Co^{2+}/Co^{3+} species in the Co_3O_4 spinel, as observed by XRD. The presence of a significant amount of surface Co^{2+} ions in the low-loaded sample could be related to a high dispersion of the cobalt oxide phase, which determines a high proportion of cobalt in the small Co_3O_4 particles to be in intimate contact with the SBA-15 support. On the other hand, the XP spectra of the Re- and Mn-promoted catalysts containing about 20 wt% Co are similar to those of the high-loaded unpromoted samples, suggesting the presence of Co_3O_4 as the main surface cobalt oxide phase.

The influence of cobalt precursor used in the impregnation step has also been investigated by XPS. As it is seen in Fig. 5 and Table 2, the Co2p transition of catalysts containing ca. 20% cobalt prepared from cobalt acetate (20CoSBA-ac) and cobalt acetylacetonate (20CoSBA-aa) appeared at higher energy (BE = 781.8–782.0 eV) than that of the equivalent catalyst prepared from cobalt nitrate (20CoSBA-n). Moreover, the former catalysts are characterized by a very high intensity of the shake-up satellite peak that unambiguously revealed the presence of Co^{2+} ions in octahedral symmetry typical of CoO [29]. These results suggest that most of the surface cobalt species in these catalysts are in the form of Co^{2+} strongly interacting with the SBA-15 surface, probably in the form of a cobalt silicate phase as observed by TEM, and discard the presence of large amounts of nanosized Co_3O_4 particles not detectable by XRD. This is further supported by the sharpness of the $Co2p_{3/2}$ peak in the acetate and acetylacetonate samples (FWHM = 3.2 and 3.3, respectively), in contrast with the higher FWHM value found for the 10CoSBA-n, as discussed above. The strong cobalt–support interaction leading to the formation of Co^{2+} species could be favored by the higher temperatures required for decomposing the organic cobalt salts as compared to cobalt nitrate, as we determined from thermogravimetric analysis (not shown).

3.1.4. Reducibility of Co species in Co/SBA-15 catalysts

3.1.4.1. X-ray photoelectron spectroscopy: reduced catalysts Fig. 6 shows the XP spectra obtained with the cobalt catalysts after in situ reduction treatment in flowing hydrogen (20% in nitrogen, 150 cm^3/min) at 673 K for 10 h. As observed in Fig. 6 and Table 2, the BE of the Co2p transition of the catalysts prepared from cobalt nitrate with low Co loading (10CoSBA-n) hardly changed after the in situ reduction treatment (BE = 781.9 eV), pointing to a low reducibility of the cobalt oxide phases present in this catalyst. For the nitrate samples with higher Co loading a

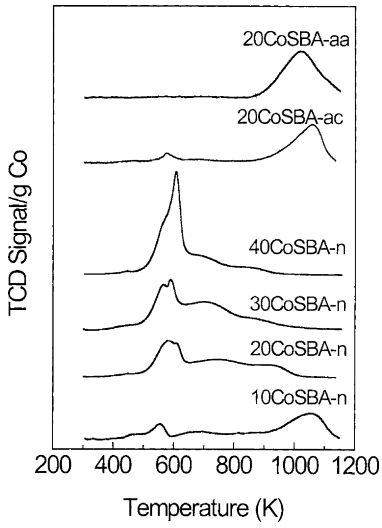

Fig. 7. TPR profiles of unpromoted Co/SBA-15 samples with different cobalt loading and prepared from different cobalt precursor salts.

peak at ca. 778 eV clearly revealed the presence of metallic cobalt [30] after the reduction step. However, the presence of other Co2p components at higher binding energies indicated that complete reduction of the cobalt oxide phases was not accomplished. For the Re- and Mn-promoted samples the Co2p peak of Co^0 also coexisted with higher energy components, reflecting again a partial reduction of cobalt oxides to metallic cobalt. The relative contribution of the Co^0 component to the $Co2p_{3/2}$ peak appeared to be higher for the Re-promoted sample as compared to the Mn-containing catalyst, indicating a greater extent of cobalt reduction in the former. Nevertheless, the reduction behavior of the different catalysts will be studied in more detail in the following section addressing the TPR results.

3.1.4.2. Temperature-programmed reduction Temperature-programmed reduction is a powerful tool to study the reduction behavior of oxidize phases; in some cases it is also possible from the reduction profiles of supported oxides to obtain useful information about the degree of interaction of the supported phase with the carrier. The influence of Co loading and cobalt precursor on the reduction behavior for the unpromoted Co/SBA-15 catalysts calcined at 573 K is shown in Fig. 7. The TPR profiles have been normalized per weight of cobalt in the catalyst to facilitate the discussion. For unpromoted samples prepared from cobalt nitrate with Co loading from ca. 20 to 40 wt% two main reduction peaks close to each other with temperature maxima at about 560–580 K ($T1_{max}$) and 590–610 K ($T2_{max}$), respectively, are observed. The first peak could be assigned to the reduction of Co_3O_4 to CoO, and the second one to the subsequent reduction of CoO to Co^0 [31,32]. The relative intensity of the second reduction peak increased with Co loading, suggesting a higher reduction degree of CoO to metallic Co with increasing the mean diameter of Co_3O_4 particles. Besides these two main reduction peaks, two broad reduction features in the temperature range of 650–800 and 800–950 K were also observed, suggesting the presence of surface Co species with different degrees of interaction with the support. The relative contribution of the species reducing at high temperature (800–950 K) to the overall reduction pattern decreased and the temperature maximum for these species shifted to lower temperatures, indicating a lower strength of interaction, with increasing Co loading. On the other hand, a significantly different reduction pattern was observed for the catalyst with ca. 10 wt% Co (10CoSBA-n). The main reduction feature for this sample was observed in the temperature range of 950–1150 K, with a maximum centered at about 1050 K. Such a high reduction temperature might be assigned to the reduction of cobalt silicate species formed during the TPR experiments by reaction of highly dispersed CoO with the siliceous SBA-15. In fact, cobalt silicates were shown to reduce at temperatures well above 723 K [33], while bulk Co_3O_4 became completely reduced at temperatures below 773 K [34,35]. Besides this high-temperature peak, a less intense reduction feature at about 560 K corresponding to the reduction of Co_3O_4 to CoO and a broad reduction in the 650–750 K temperature range were also observed. All these features suggest that most of the Co in the calcined 10CoSBA-n sample was strongly interacting with the SBA-15 support, as also evidenced from XPS data.

Besides Co loading, the nature of the cobalt precursor used in the impregnation step also had a marked influence on the reduction behavior of Co/SBA-15 catalysts. The reduction profiles of the catalysts loaded with ca. 20 wt% Co and prepared from cobalt acetate (20CoSBA-ac) and cobalt acetylacetonate (20CoSBA-aa) are also shown in Fig. 7. As observed, these two samples presented a reduction behavior significantly different from that of the sample prepared from cobalt nitrate and having similar Co loading (20CoSBA-n). The TPR profile of the 20CoSBA-ac sample is characterized by a small peak at about 575 K attributed to the reduction of Co_3O_4 to CoO, and a large reduction peak centered at about 1060 K, while that of 20CoSBA-aa only showed an intense reduction peak centered at ca. 1020 K. As discussed above, the high-temperature peak could be assigned to the reduction of cobalt silicate species (observed by TEM in the acetate sample) probably formed by reaction of Co^{2+} species strongly interacting with the SBA-15 support, as seen by XPS. Such a strong interaction could be favored by a high dispersion of the cobalt phases and the higher temperatures required for the decomposition of the organic cobalt salts as compared to the nitrate precursor. Sun et al. [27] also observed that Co in a Co/SiO_2 (10 wt% Co) catalyst prepared from cobalt acetate started to be reduced at temperatures above 1000 K. Then, we suggest that the cobalt silicate phase observed in these catalysts could be formed during the calcination of the catalysts rather than during the reduction process, as probably occurs for the low-loaded 10 wt% Co sample prepared from cobalt nitrate.

Finally, the effect of Re and Mn promoters on the reduction behavior of Co/SBA-15 catalysts is presented in Fig. 8.

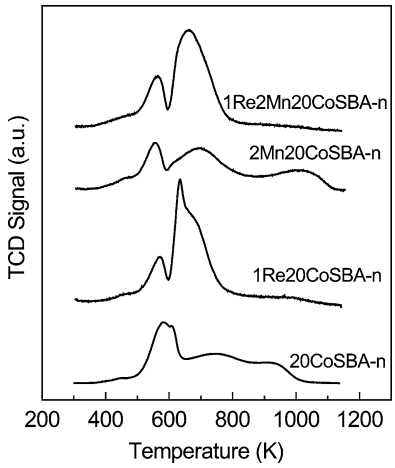

Fig. 8. TPR profiles of unpromoted and Re- and Mn-promoted Co/SBA-15 catalysts with ca. 20 wt% Co loading.

The catalyst promoted with about 1 wt% Re showed a first reduction peak with a maximum at ca. 570 K and a more intense reduction peak at ca. 635 K with a pronounced shoulder at ca. 675 K. By comparing the reduction profile of this sample with that of the unpromoted catalyst with similar Co loading, it becomes evident that the addition of small amounts of Re hardly affected the reducibility of Co oxide species reduced at low temperatures (ca. 570–580 K) but it significantly improved the reducibility of those species that had a stronger interaction with the support [24]. This effect has been ascribed to H_2 spilled over from metallic Re to the Co species interacting with the support [24,36]. On the other hand, it can be seen in Fig. 8 that the addition of Mn had little effect on the reduction of Co_3O_4 to CoO (a slight shift in $T1_{max}$ from ca. 580 to 555 K), but it hindered the second reduction step (from CoO to Co^0), as observed from the broad and intense reduction peak with $T2_{max}$ at ca. 695 K. Moreover, a broad reduction feature in the temperature range of ca. 900–1100 K with a maximum at about 1010 K was also observed, indicating the formation of hardly reducible cobalt silicate species, as found in the low-loaded sample prepared from cobalt nitrate and those obtained from the acetate and acetylacetonate precursors. Yin et al. [12] also observed that the addition of 2 wt% Mn to a mesoporous 15% Co/HMS catalyst made the reduction process of Co_3O_4 to Co^0 more difficult as compared to the unpromoted sample. The lower reducibility of Co oxide after addition of Mn was attributed to a partial segregation of Co_3O_4 crystallites favoring Co–support interactions as well as to a possible interaction of MnO with Co oxides [12]. Unfortunately, in that work the TPR process was stopped at 773 K and thus the high-temperature reduction peak above 1000 K was not observed. In our case, the XRD results showed the formation of very small Co_3O_4 crystallites with an average diameter of 5.9 nm upon the addition of Mn (Table 2). Then, the interaction of such a highly dispersed cobalt oxide particles could favor the formation of the cobalt silicates during the reduction process. Finally, it is also seen in Fig. 8 that the reduction profile of the sample promoted with both Re and Mn was similar to that of the Re-promoted sample. This suggests that the presence of Re facilitated the reduction of the less reducible Co species interacting with MnO and the SBA-15 support.

The extent of Co reduction estimated from the amount of H_2 consumed during TPR experiments after reducing the samples at 673 K for 10 h is given in Table 2. The extent of reduction of unpromoted Co/SBA-15 samples prepared from cobalt nitrate increased from 27 to 89% when increasing the Co loading from ca. 10 to 40 wt%. In a previous characterization study, Khodakov et al. [37,38] showed that the hydrogen reduction properties of supported cobalt oxide particles depended on the size of the Co_3O_4 crystallites, with larger particles being much easily reduced. This finding is in agreement with the observed increase of reducibility with increasing Co_3O_4 particle size in the unpromoted xCo/SBA-n series with different Co loading. As expected from the TPR profiles discussed above, at similar Co loading the extent of Co reduction was much lower for the samples impregnated with cobalt acetate (28%) and acetylacetonate (12%). Finally, it is seen that the amount of reduced Co increased from 62 to 83% upon addition of Re, while it decreased to 40% for the Mn-promoted sample. The extent of Co reduction for the sample promoted with both Re and Mn was similar to that of the Re-promoted catalyst (85%). These trends are in good agreement with the changes in the reduction profiles discussed above. It can also be seen in Table 2 that at comparable Co loading (ca. 20 wt%) the extent of reduction of Co supported on amorphous silica ($20CoSiO_2$) was higher (89%) than when supported on the mesoporous SBA-15 material (62%). This fact can be related with the larger particle size of Co_3O_4 in the former catalyst (Table 2).

3.2. Catalytic results for the FTS reaction

3.2.1. Activity of Co/SBA-15 catalysts

The catalytic activity of the different Co/SBA-15 catalysts was studied in a fixed-bed reactor under typical FTS conditions: 493 K, 20 bar, $H_2/CO = 2$, and GHSV of 13.5 l(NTP)/(g_{cat} h). Under these conditions the conversion of CO gradually decreased during the first 10–15 h and then a pseudo-stationary state was observed, the decrease being more pronounced for the most active catalysts (not shown). The activity and selectivity values reported here correspond to the period of pseudo-stationary behavior. The catalytic results are summarized in Table 3. For unpromoted catalysts prepared from cobalt nitrate the conversion of CO passed a maximum at a Co loading of ca. 30 wt%. In principle, the activity of reduced Co catalysts should be proportional to the concentration of surface Co^0 sites. The maximum activity obtained thus reflected the inverse trends of cobalt dispersion and extent of reduction observed when increasing Co loading (Table 2). Therefore, the maximum concentration of surface Co^0 sites is achieved for the 30 wt% Co sample presenting a good dispersion and high reducibility. As

Table 3
FTS results for Co/SBA-15 catalysts

Catalyst	CO conversion	Selectivity[a] (%C)			Hydrocarbon distribution (%C)			C_{10+}/C_{5+}	Olefins/RH[b]	α[c]
	(%)	CO_2	ROH	RH	C_1	C_2–C_4	C_{5+}	ratio	(%C)	
10CoSBA-n	13.2	6.3	10.9	82.8	28.4	25.3	46.3	0.63	13.8	0.86
20CoSBA-n	23.1	1.2	5.0	93.8	19.5	15.8	64.7	0.58	10.5	0.87
30CoSBA-n	33.1	1.1	3.3	95.6	21.3	15.5	63.2	0.54	12.9	0.86
40CoSBA-n	30.1	0.7	3.9	95.4	18.5	14.8	66.7	0.63	17.8	0.87
20CoSBA-ac	5.5	6.2	10.6	83.2	33.5	30.9	35.6	0.57	19.0	0.85
20CoSBA-aa	5.0	9.6	19.1	71.3	56.2	42.1	1.7	-	9.8	0.30
1Re20CoSBA-n	43.0	1.3	3.7	95.0	14.1	11.7	74.2	0.70	8.3	0.87
2Mn20CoSBA-n	13.2	3.4	16.3	80.3	19.2	36.6	44.2	0.37	29.6	0.78
1Re2Mn20CoSBA-n	11.5	4.6	17.1	78.3	20.4	35.4	44.2	0.36	28.7	0.77
$20CoSiO_2$	17.7	6.0	7.2	86.8	17.9	19.1	63.0	0.70	12.2	0.83

Reaction conditions: 493 K, 20 bar, $H_2/CO = 2$, GHSV = 13.5 l(NTP)/(g_{cat} h).
[a] ROH, alcohols; RH, hydrocarbons.
[b] Percentage of α-olefins in the hydrocarbon fraction.
[c] Chain-growth probability obtained from the ASF plot in the C_8–C_{14} hydrocarbons range.

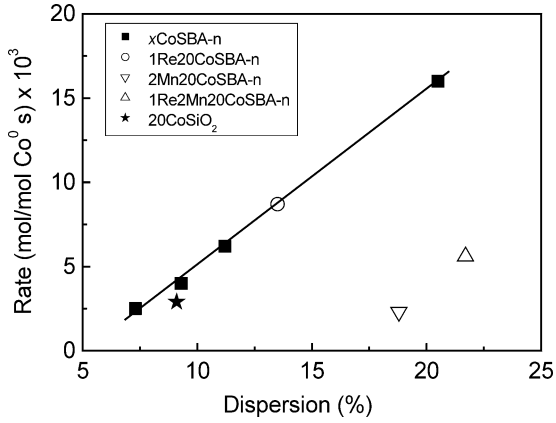

Fig. 9. FTS reaction rate based on reduced cobalt as a function of Co^0 dispersion.

observed in Fig. 9, the steady-state rate of CO conversion calculated on the basis of reduced cobalt (total Co content x extent of reduction at 673 K) increased linearly with Co^0 dispersion for the series of unpromoted samples prepared from Co nitrate. This trend implies a constant intrinsic activity of Co irrespective of Co content and particle size (i.e., dispersion). By working at atmospheric pressure and differential conditions, Khodakov et al. [15] observed an increase of the turnover when increasing the particle size of cobalt supported on mesoporous silicas of different pore size. Our results, however, are in agreement with those of Iglesia et al. [11], who reported a constant turnover for Co-based FTS catalysts when working under typical FTS conditions favoring high C_{5+} selectivities, as in the present work. It can also be seen in Table 3 that at similar Co loading the catalyst based on the mesoporous SBA-15 support is about 1.5 times more active per weight of total cobalt than that based on amorphous silica. This higher activity can be related with a higher dispersion of cobalt on the high surface area mesoporous support, even thought the reducibility of cobalt oxides was somewhat larger for the silica-supported catalyst (Table 2). In fact, the reaction rate per amount of reduced cobalt for the $20CoSiO_2$ catalyst was very close to that of unpromoted xCoSBA-n samples (Fig. 9), suggesting a similar intrinsic activity of Co^0 in both supports.

As observed in Table 3 the catalysts prepared from cobalt acetate and acetylacetonate precursors were much less active (CO conversion of 5.5 and 5.0%, respectively) than that prepared from cobalt nitrate at similar Co lading. Such a low activity can be related to the low reducibility of cobalt species in the former catalysts, probably in the form of cobalt silicates as discussed before. After the addition of small amounts of Re (ca. 1 wt%) the conversion of CO was significantly increased from 23 to 43% (Table 3), which can be ascribed to the higher reducibility and slightly better dispersion of cobalt in this sample as compared to the unpromoted one. Indeed, the reaction rate per reduced cobalt obtained for 1Re20CoSBA-n was that expected for the level of Co dispersion achieved in this sample (Fig. 9), indicating that the intrinsic activity of Co was not modified upon the addition of Re. By contrast, results in Table 3 show that the CO conversion of the Mn-containing catalysts (2Mn20CoSBA-n and 1Re2Mn20CoSBA-n) was much lower than that of the unpromoted catalyst with similar Co loading. Yin et al. [12] also observed a significant reduction of the CO conversion from ca. 72 to 40% at 493 K upon addition of 2 wt% Mn to a 15% Co/HMS catalyst, even though the activity of the Mn-promoted sample approached that of the unpromoted one at higher reaction temperatures. The relatively low activity obtained for the Mn-promoted catalysts is surprising if one takes into account their high Co^0 dispersion and reducibility. In fact, the rate of CO conversion per reduced Co for the Mn-promoted catalysts was much lower than that of the unpromoted 10CoSBA-n sample having similar dispersion (Fig. 9), pointing to a lower intrinsic activity of Co^0 in the former catalysts. The characterization data obtained in this work do not offer a clear explanation for these results, although a close interaction of cobalt with manganese species might contribute to the low activity of the Mn-promoted catalysts. In this sense, in a recent in situ diffuse reflectance

FTIR study using CO and $CO + H_2$ probe molecules, Jiang et al. [39] observed a change in the adsorption properties of surface Co^0 species induced by the presence of Mn in precipitated Co/Mn catalysts that resulted in an initially lower activity for the FTS reaction.

3.2.2. Product selectivity

The selectivity (on a carbon basis) to the different FTS products obtained for the unpromoted and promoted Co/SBA-15 catalysts is also presented in Table 3. Concerning the series of samples prepared from Co nitrate, it can be seen that the unpromoted *x*CoSBA-n catalysts with ca. 20–40 wt% Co loading presented a high selectivity toward hydrocarbons (ca. 94–96%), and low selectivity toward alcohols (ca. 3–5%) and CO_2 (ca. 1%) reflecting a low activity for the competitive water-gas shift reaction (WGS: $CO + H_2O \rightarrow CO_2 + H_2$) typically observed for Co-based FTS catalysts. However, a distinct selectivity is observed for the low-loaded 10CoSBA-n sample. This catalyst produced more CO_2 (ca. 6%) and alcohols and less hydrocarbons than those with higher Co content. Moreover, a higher concentration of light products (methane, C_2–C_4) within the hydrocarbon fraction was obtained for the low-loaded catalyst. The chain growth probability, α, obtained from the slopes of the Anderson–Shultz–Flory (ASF) plots in the C_8–C_{14} hydrocarbon range (0.86–0.87) did not change with Co loading. As observed in Table 3, the product selectivities obtained for the acetate and acetylacetonate catalysts were similar to those of the low-loaded 10CoSBA-n sample prepared from cobalt nitrate, i.e., a relatively high selectivity to CO_2, alcohols, and methane. Selectivities to these products were particularly high for the acetylacetonate 20CoSBA-aa sample, for which the concentration of methane in the hydrocarbon fraction reached a value of ca. 56% with a very low chain growth probability ($\alpha = 0.30$). High methane selectivities have also been reported in the literature for low-loaded Co catalysts presenting high dispersion and low reducibility [22]. This effect was attributed to the presence of unreduced cobalt oxides catalyzing the WGS reaction, thus increasing the effective H_2/CO ratio at the catalyst surface. The local increase of the H_2/CO ratio near the surface Co^0 sites would favor hydrogenation of the adsorbed species leading to higher methane selectivities. Khodakov et al. [15] found an inverse relationship between methane selectivity and the overall extent of Co reduction in a series of cobalt–supported mesoporous silicas with different pore sizes. However, these authors did not observe significant formation of CO_2 in their catalysts and thus the higher methane selectivities were ascribed to the presence of either unreduced cobalt species or to small cobalt particles, rather than to a higher activity for the WGS reaction. By contrast, in our study we observed a general parallelism between the selectivities to methane and CO_2, suggesting that the higher methane selectivity displayed by well-dispersed low-reducible catalysts could be due, at least in part, to a higher extent of the WGS reaction occurring on unreduced Co species.

The influence of promoters on product selectivity is also shown in Table 3. The addition of Re reduced the selectivity to methane and favored the formation of long-chain *n*-paraffins (C_{10+}) with respect to the unpromoted catalyst. The increase in selectivity toward higher hydrocarbons observed for the Re-promoted catalyst was accompanied by a decrease of the olefin content in the hydrocarbon fraction. This result reflects a higher readsorption of the α-olefins which thus could participate in the chain-growing process favoring the formation of high molecular weight products. A higher readsorption of α-olefins can be originated by an increase in the density of surface Co^0 sites caused by the higher reducibility and dispersion of the Re-promoted catalyst, as suggested by Iglesia et al. [40] for Co–Ru catalysts. On the other hand, the Mn-promoted catalysts produced more alcohols ($S_{ROH} = 16$–17%), slightly more CO_2, and less hydrocarbons than the unpromoted one with similar Co loading. Moreover, the product distribution within the hydrocarbon fraction in the Mn-containing catalysts was shifted toward the formation of lighter products (more C_2–C_4, lower C_{10+}/C_{5+} ratio and lower α). Recently, Yin et al. [12] also observed a significant increase of the methane selectivity and a decrease of C_{5+} products upon addition of 2 wt% Mn to a Co/HMS catalyst at a reaction temperature of 493 K. Moreover, the concentration of olefins in the hydrocarbon fraction was much higher for the Mn catalysts (about 30% olefins). An enhanced formation of olefins, mainly in the C_2–C_4 range, has been generally reported in the literature for Mn-promoted Co- and Fe-based FTS catalysts [41–46].

Finally, no significant differences in product selectivity were found for the SBA-15 and SiO_2-supported catalysts having similar Co loading (ca. 20 wt%) and prepared from cobalt nitrate precursor, though the latter produced a higher concentration of C_{10+} *n*-paraffins in the C_{5+} fraction.

4. Conclusions

The physico-chemical and catalytic properties for the Fischer–Tropsch synthesis reaction of mesoporous SBA-15- (pore diameter of 10.0 nm) supported cobalt catalysts have been investigated as a function of cobalt loading, cobalt precursor, and addition of promoters (Re, Mn). Calcined Co/SBA-15 catalysts prepared from Co(II) nitrate with cobalt loadings of 10–40 wt% contained Co_3O_4 as the only crystalline phase. The mesoporous structure of the SBA-15 support was preserved after cobalt impregnation and calcination at 573 K, as observed by TEM. The dispersion of Co^0, calculated from the average particle size of Co_3O_4, decreased from ca. 20 to 7% and the extent of cobalt reduction at 673 K, determined from TPR experiments, increased from 27 to 89% when increasing Co loading from ca. 10 to 40 wt%. A maximum CO conversion was obtained for the catalyst loaded with ca. 30 wt% Co presenting the highest density of surface Co^0 sites, as determined from the total Co content, Co^0 dispersion, and degree of reduction

at 673 K. However, the intrinsic activity of Co^0 (turnover) remained constant in the range of cobalt loading studied. Product selectivities were also influenced by Co loading. The formation of C_{5+} hydrocarbons (mainly *n*-paraffins) was favored over Co/SBA-15 catalysts presenting high reducibility, while the product distribution shifted toward the formation of lighter hydrocarbons (methane, C_2–C_4) for the less reducible low-loaded (ca. 10 wt% Co) sample.

The addition of small amounts of rhenium (ca. 1 wt% Re) to a 20 wt% Co/SBA-15 catalyst promoted the reduction of the less-reducible cobalt species which had a stronger interaction with the support, as observed by TPR, without significantly affecting cobalt dispersion. Consequently, the catalytic activity per weight of total cobalt of the Re-promoted sample increased, though the turnover of the accessible Co^0 sites was not altered with respect to the unpromoted catalyst. Moreover, the higher density of reduced Co sites in the Re-promoted catalyst favored the formation of long-chain *n*-paraffins (C_{10+}) while the selectivity to methane decreased. On the other hand, promotion with ca. 2 wt% Mn significantly improved the dispersion of Co^0 from ca. 11% for the unpromoted catalyst (ca. 20 wt% Co loading) to 22%. However, the increase in dispersion and the presence of Mn favored a strong interaction of cobalt oxides with the support and possibly also with the MnO phases producing catalysts that were about 50% less active than the unpromoted one. Furthermore, the product distribution obtained for the Mn-containing catalysts was characterized by a higher formation of alcohols (ca. 16–17% selectivity), a lower selectivity to C_{5+} products within the hydrocarbon fraction, and an increased olefinicity, mainly in the C_2–C_4 range.

A very high cobalt dispersion was observed for Co/SBA-15 catalysts containing ca. 20 wt% prepared from organic cobalt precursors (acetate, acetylacetonate). Most of the cobalt species in these catalysts were strongly interacting with the support, probably forming cobalt silicates, as evidenced by XPS and TEM, and could be reduced only at temperatures above 1000 K. The presence of large amounts of unreduced cobalt phases in the acetate and acetylacetonate derived catalysts lead to very low FTS activities and high methane selectivities.

Finally, at similar Co loading (ca. 20 wt% Co) Co/SBA-15 was found to be about 1.5 times more active (per weight of total cobalt) than a Co/SiO_2 sample, owing to a better dispersion of the cobalt phases in the mesoporous catalyst. Surface Co^0 sites supported on both SBA-15 and SiO_2 carriers displayed, however, comparable intrinsic activities. Product selectivities were also comparable, though a slightly higher selectivity to C_{10+} hydrocarbons was found for the silica-supported sample.

Acknowledgments

Financial support by the Comisión Interministerial de Ciencia y Tecnología (CICYT) of Spain (Project MAT2001-2726) is gratefully acknowledged. C.L. acknowledges the Ministerio de Ciencia y Tecnología of Spain for a Ph.D. scholarship.

References

[1] T.H. Fleisch, R.A. Sills, M.D. Briscoe, J. Nat. Gas Chem. 11 (2002) 1.
[2] B. Lutz, Hydrocarbon Eng. 6 (2001) 23.
[3] A.M. Thayer, Chem. Eng. News March 13 (2000) 20.
[4] G.P. Van der Laan, A.A.C.M. Beenackers, Catal. Rev.-Sci. Eng. 41 (1999) 255.
[5] J.H. Gregor, Catal. Lett. 7 (1990) 317.
[6] M.A. Vannice, J. Catal. 50 (1977) 228.
[7] M.E. Dry, Catal. Today 6 (1990) 183.
[8] E. Iglesia, Appl. Catal. A 161 (1997) 50.
[9] C.A. Chanenchuk, I.C. Yates, C.N. Satterfield, Energy Fuels 5 (1991) 848.
[10] H. Schultz, Appl. Catal. A 186 (1999) 3.
[11] E. Iglesia, S.L. Soled, R.A. Fiato, J. Catal. 137 (1992) 212.
[12] D. Yin, W. Li, W. Yang, H. Xiang, Y. Sun, B. Zhong, S. Peng, Micropor. Mesopor. Mater. 47 (2001) 15.
[13] J. Panpranot, J.G. Goodwin Jr., A. Sayari, Catal. Today 77 (2002) 269.
[14] Y. Wang, M. Noguchi, Y. Takahashi, Y. Ohtsuka, Catal. Today 68 (2001) 3.
[15] A.Y. Khodakov, A. Griboval-Constant, R. Bechara, V.L. Zholobenko, J. Catal. 206 (2002) 230.
[16] A. Griboval-Constant, A.Y. Khodakov, R. Bechara, V.L. Zholobenko, Stud. Surf. Sci. Catal. 144 (2002) 609.
[17] A.Y. Khodakov, R. Bechara, A. Griboval-Constant, Stud. Surf. Sci. Catal. 142 (2002) 1133.
[18] D. Zhao, J. Feng, Q. Huo, N. Melosh, G.H. Fredrickson, B.F. Chmelka, G.D. Stucky, Science 279 (1998) 548.
[19] D.Y. Zhao, Q.S. Huo, J.L. Feng, B.F. Chmelka, G.D. Stucky, J. Am. Chem. Soc. 120 (1998) 6024.
[20] D. Zhao, J. Sun, G. Li, G.D. Stucky, Chem. Mater. 12 (2000) 275.
[21] B.D. Cullity, Elements of X-Ray Diffraction, Addision–Wesley, London, 1978.
[22] R.C. Reuel, C.H. Bartholomew, J. Catal. 85 (1984) 63.
[23] R.D. Jones, C.H. Bartholomew, Appl. Catal. 39 (1988) 77.
[24] G. Jacobs, T.K. Das, Y. Zhang, J. Li, G. Racoillet, B.H. Davis, Appl. Catal. A 233 (2002) 263.
[25] Z. Luan, M. Hartmann, D. Zhao, W. Zhou, L. Kevan, Chem. Mater. 11 (1999) 1621.
[26] Z. Luan, E.M. Maes, P.A.W. van der Heide, D. Zhao, R.S. Czernuszewicz, L. Kevan, Chem. Mater. 11 (1999) 3680.
[27] S. Sun, N. Tsubaki, K. Fujimoto, Appl. Catal. A 202 (2000) 121.
[28] Y. Brik, M. Kacimi, M. Ziyad, F. Bozon-Verduraz, J. Catal. 202 (2001) 118.
[29] V.I. Nefedov, M.N. Firsov, I.S. Shaplygin, J. Electron Spectrosc. Related Phenom. 26 (1982) 65.
[30] J.S. Hammond, N. Winograd, J. Electroanal. Chem. 78 (1977) 55.
[31] P. Arnoldy, J.A. Moulijn, J. Catal. 93 (1985) 38.
[32] B. Viswanathan, R. Gopalakrishnan, J. Catal. 99 (1986) 342.
[33] B. Sexton, A. Hughes, T. Turney, J. Catal. 97 (1986) 390.
[34] S. Bessell, Appl. Catal. A 96 (1993) 253.
[35] G. Sewell, C. O'Connor, E. van Steen, Appl. Catal. A 125 (1995) 99.
[36] S. Vada, A. Hoff, E. Adnanes, D. Schanke, A. Holmen, Top. Catal. 2 (1995) 155.
[37] A.Y. Khodakov, J. Lynch, D. Bazin, B. Rebours, N. Zanier, B. Moisson, P. Chaumette, J. Catal. 168 (1997) 16.
[38] A.Y. Khodakov, A. Griboval-Constant, R. Bechara, F. Villain, J. Phys. Chem. B 105 (2001) 9805.
[39] M. Jiang, N. Koizumi, T. Ozaki, M. Yamada, Appl. Catal. A 209 (2001) 59.

[40] E. Iglesia, S.L. Soled, R.A. Fiato, G.H. Via, Stud. Surf. Sci. Catal. 81 (1994) 433.
[41] K.B. Jensen, F.E. Massoth, J. Catal. 92 (1985) 98.
[42] J. Barrautl, C. Renard, Appl. Catal. 14 (1985) 133.
[43] M. van der Riet, G.J. Hutchings, R.G. Copperthwaite, J. Chem. Commun., Chem. Commun. (1986) 798.
[44] G.J. Hutchings, R.G. Copperthwaite, M. van der Riet, Top. Catal. 2 (1995) 163.
[45] S.E. Colley, R.G. Copperthwaite, G.J. Hutchings, N.J. Coville, J. Catal. 134 (1992) 186.
[46] A.A. Adesina, Appl. Catal. A 138 (1996) 345.